INSTITUTE OF PHYSICS PUBLISHING PLASMA PHYSICS AND CONTROLLED FUSION

Plasma Phys. Control. Fusion **46** (2004) 1259–1270 PII: S0741-3335(04)68225-X

Edge stability analysis of high β_p plasmas

S Saarelma[1] **and S Günter**[2]

[1] Helsinki University of Technology, Euratom-TEKES Association, FIN-02015 HUT, Finland
[2] Max-Planck-Institut für Plasmaphysik, EURATOM Association, Boltzmannstr. 2, D-85748 Garching, Germany

E-mail: samuli.saarelma@hut.fi

Received 2 September 2003
Published 24 June 2004
Online at stacks.iop.org/PPCF/46/1259
doi:10.1088/0741-3335/46/8/007

Abstract

An MHD stability analysis of the edge plasma shows that in highly triangular plasmas, the increasing global β_p has a stabilizing effect on the low-n instabilities that trigger edge localized modes (ELMs). The improved stability allows the access of higher edge pressure gradients before the ELM is triggered. At the same time, the edge plasma moves closer to the high-n ballooning mode stability boundary. The stability changes can explain why the high value of β_p helps to access smaller ELMs.

(Some figures in this article are in colour only in the electronic version)

1. Introduction

In a tokamak fusion reactor, high power load on divertor plates can cause unacceptable erosion and should therefore be avoided. High confinement (H-mode) plasmas are usually characterized by ELMs that release plasma particles and energy from inside the separatrix into the scrape-off-layer (SOL) in short ($t < 1$ ms) bursts. These intense energy bursts are especially detrimental to the divertor. The erosion is reduced if the ELMs are completely eliminated or at least their amplitude lowered.

The most dangerous ELMs are Type I or 'giant' ELMs that release several per cent of the plasma energy in each burst. Operation with smaller Type III ELMs significantly reduces divertor loads, but unfortunately the confinement in plasmas with Type III ELMs is worse than in those with Type I ELMs. Most probably, Type III ELMs are not a suitable operating regime for a fusion reactor. Compared with the Type I ELMs, the Type II or 'grassy' ELMs have significantly lower energy loss per ELM, while the plasma confinement is maintained at the same level. They offer the possibility of operating the tokamak fusion reactor with good edge confinement and small ELMs.

Connor *et al* [1] have proposed a model where Type I ELMs are caused by a coupled peeling–ballooning instability driven by the interplay between the edge pressure gradient and the edge current. The model has been found to produce results for ASDEX Upgrade Type I

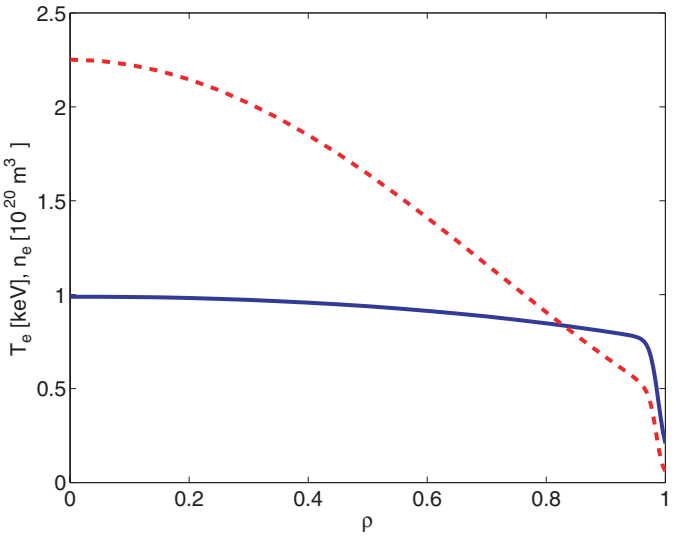

Figure 1. The density (——) and temperature (- - - -) profiles as a function of normalized radius in ASDEX Upgrade shot 15865 at 5.0 s.

ELMy plasmas in agreement with the experimental observations [2]. Recently, on JT-60U, it has been observed that the edge stability is improved in high triangularity plasmas, when β_p is increased [3]. Additionally, high β_p is found to facilitate the access to plasmas where the giant Type I ELMs are replaced by smaller grassy ELMs [4]. In this paper, we use the ELM model to study the edge stability changes when the global β_p is increased. Following the model, in the stability analysis, we concentrate on low- to intermediate-n peeling–ballooning modes and high-n ballooning modes, because, in addition to ASDEX Upgrade, these instabilities are found to explain the Type I ELM triggering DIII-D and JT-60U [5] as well.

2. Investigated plasma equilibria

We investigate the effect of the core β_p on the edge stability by starting from an equilibrium of an experimental plasma that displays Type I ELMs. We artificially increase the core pressure, but keep the edge profiles unchanged. We also vary the shape of the plasma to see if the effect of the increased β_p depends on the plasma shape. Figure 1 shows the profiles for electron temperature and density as a function of $\rho = \sqrt{\psi}_N$ where ψ_N is the normalized poloidal flux. The profiles are taken from ASDEX Upgrade shot #15865 at 5.0 s and smoothed for the equilibrium reconstruction. For ions, we assume $T_\mathrm{i} = T_\mathrm{e}$. In this shot, the plasma current is 0.8 MA and the toroidal magnetic field is 2 T. The geometric major radius is 1.67 m and the minor radius is 0.50 m. The triangularity of the plasma is 0.42 and elongation 1.69. The global β_p in this discharge is 1.1.

The edge stability is determined by the pressure gradient, the magnetic shear and the current gradient. These are connected so that the magnetic shear depends mainly on the current density—the higher the current density, the lower the shear. At the edge of the plasma, the bootstrap current dominates the inductively driven current because of the very steep pressure gradient of the edge transport barrier. We include the bootstrap current in the equilibrium calculation using an analytical formula for the flux averaged parallel bootstrap current $\langle \boldsymbol{j} \cdot \boldsymbol{B} \rangle / (\mu_0 J)$ given by Sauter *et al* [6]. Figure 2 shows the pressure gradient and the

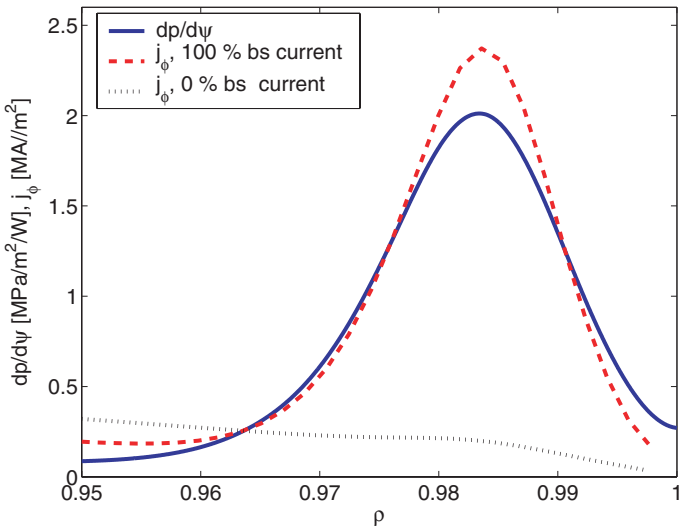

Figure 2. The pressure gradient for the plasma with no ITB and the current density with and without bootstrap current included in the equilibrium reconstruction.

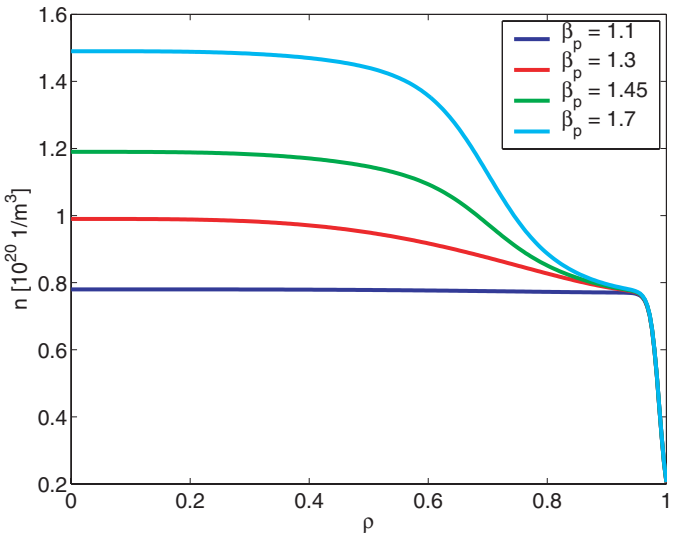

Figure 3. The density profiles used in the β_p scan.

flux surface averaged toroidal current density with and without bootstrap current near the edge. In the stability analysis, we vary the amount of the bootstrap current that is taken into account in the equilibrium reconstruction. This can be interpreted as the gradual current build-up prior to an ELM.

We modify β_p by creating an artificial internal transport barrier (ITB) in the density profile. The effect on the edge stability is the same, if instead the temperature profile is modified. The shape of the plasma is kept unchanged and the magnetic axis moves outwards according to the Shafranov shift. The density profiles used and the corresponding β_p values are shown in figure 3.

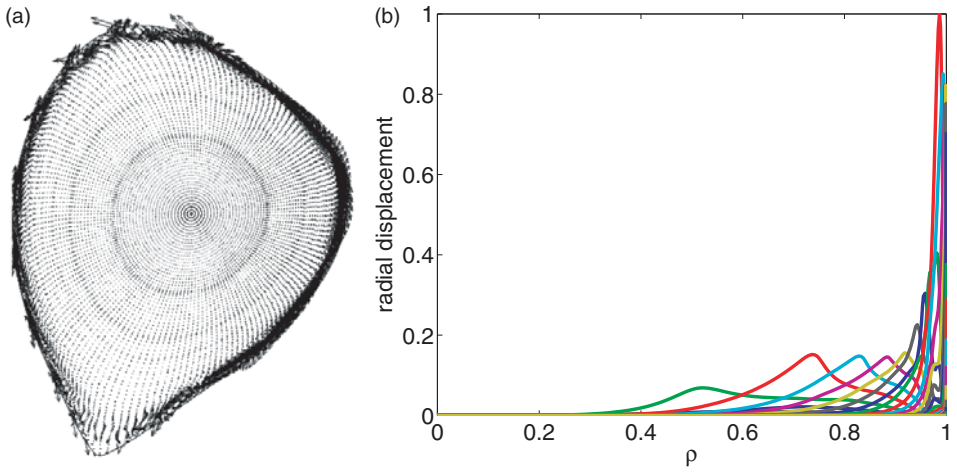

Figure 4. (*a*) The plasma perturbation of the $n = 3$ peeling–ballooning mode for ASDEX Upgrade shot #15865 at 5.0 s. (*b*) Fourier decomposition of the radial perturbation, $X = \xi \cdot \nabla\psi$.

3. Stability analysis

We analyse the edge plasma stability changes for both low- to intermediate-n peeling–ballooning modes and high-n ballooning modes as β_p is increased. In ASDEX Upgrade, $n = 3$ precursors have been observed for Type I ELMs [8]. Therefore, the main emphasis here is on the analysis of the changes in the behaviour of the $n = 3$ mode with the change in β_p.

3.1. Low- to intermediate-n stability at high triangularity

In the ideal MHD stability analysis for the low- to intermediate-n ($1 \leqslant n \leqslant 8$) modes we use the GATO code [7]. Computational limitations restrict us from studying even higher mode numbers. The conductive wall is assumed to be far from the plasma. Since the instabilities are very localized, the wall has a very small effect on them in any case and no change in stability was found for a few selected cases that were studied with a realistic ASDEX Upgrade wall. GATO cannot handle a separatrix in the plasma. Therefore, we cut away 0.02% of the flux from the separatrix. We investigated the effect of the cut-off and found that 1% of the flux had to be cut from the plasma to see changes in the stability. It is, therefore, unlikely that the stability boundaries presented here are significantly different in a true separatrix plasma.

In the stability analysis, we increase β_p by raising the core pressure. For each value of β_p we also vary the amount of bootstrap current that was included in the equilibrium reconstruction to find the stability boundary. With fixed edge temperature and density profiles, this bootstrap current fraction (percentage of the full bootstrap current given by the formula in [6]) determines the current in the edge region.

The $n = 1$ and $n = 2$ modes are stable in the entire investigated range of equilibria with the exception of the lowest value of β_p with the highest value of current. Therefore, they are excluded from the results. The mode structure of an $n = 3$ peeling–ballooning mode for $\beta_p = 1.1$ and 100% bootstrap current fraction is shown in figure 4. A comparison between $n = 3$ and $n = 8$ mode widths is shown in figure 5, where the sums over all the Fourier components of the radial displacement are plotted. As can be seen, the mode structure gets gradually narrower with increasing mode number. In a convergence test, we found that a grid

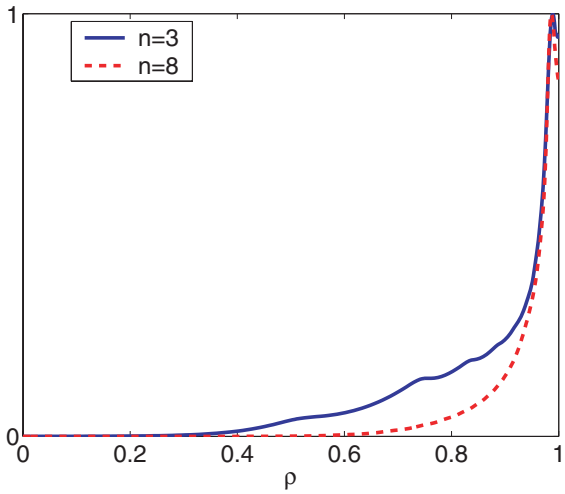

Figure 5. The normalized sum over Fourier components of the radial displacement $X = \xi \cdot \nabla\psi$ for $n = 3$ (——) and $n = 8$ (- - - -) modes.

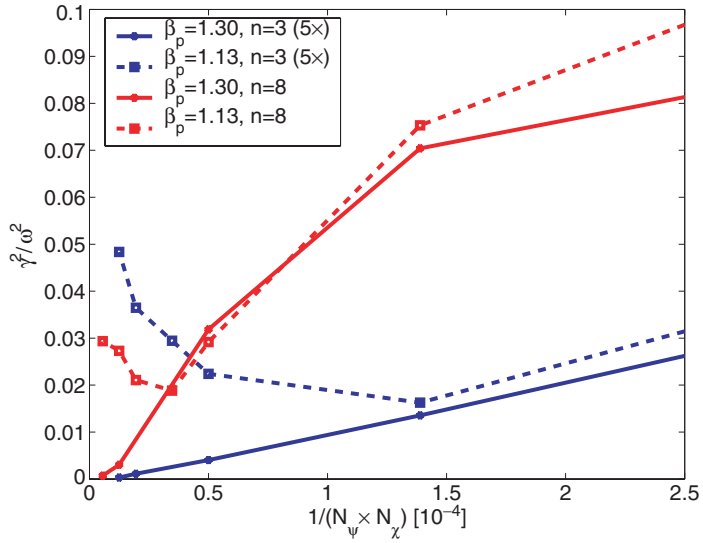

Figure 6. The convergence study for two plasmas and two mode numbers showing the growth rate as a function of the inverse grid size $1/(N_\psi \times N_\chi)$. The growth rates of the $n = 3$ mode are multiplied by 5.

of $N_\psi \times N_\chi = 200 \times 400$ flux surfaces and poloidal angles for $n = 3$ and 300×600 for $n = 8$ were sufficient to determine the stability. The convergence of the $n = 3$ and $n = 8$ modes is illustrated in figure 6 where the growth rates are plotted as a function of the grid size for two plasmas, one that is stable and the other that is unstable against both modes.

We find the driving mechanism of the instability by comparing two equilibra with different edge pressure gradients. The reference equilibrium (profiles shown in figure 1) has the maximum flux surface averaged pressure gradient of 520 kPa m^{-1}. In the other equilibrium, we steepen the temperature gradient in the edge region so that the maximum flux surface

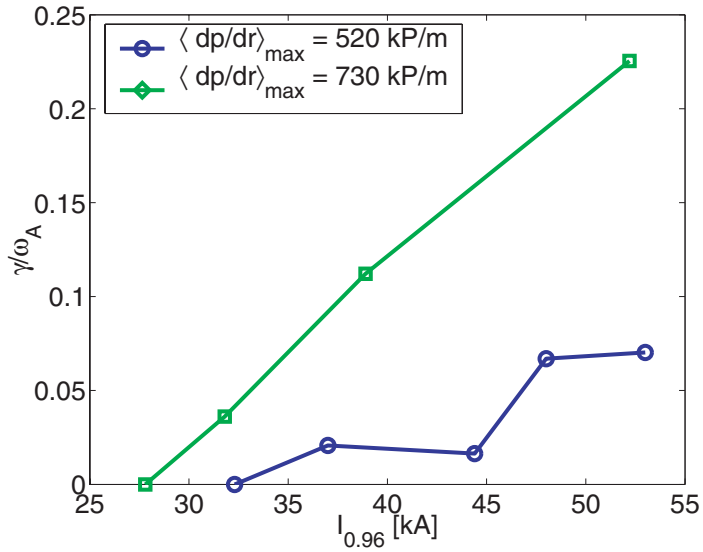

Figure 7. The growth rate of the $n = 3$ peeling–ballooning mode as a function of toroidal current in the pedestal region ($\rho > 0.96$) for two values of maximum pedestal gradient.

pressure gradient is increased by 40% to 730 kPa m^{-1}. The core profiles and global values of β_p are identical. We compare the equilibria by varying the edge current and analysing the stability against the $n = 3$ mode. The result of the stability comparison is illustrated in figure 7. It can be seen that both the increase of the edge current and the increase of pressure gradient can destabilize the edge plasma. Therefore, the instability is driven by both the pressure gradient and the current density.

When the core pressure and β_p increase, the plasma equilibrium is altered. The bootstrap current in the ITB gradient region increases, and of course, with a sufficiently large increase, it affects the global stability of the plasma, but with a modest increase of β_p, it has little direct effect on the local edge stability. The effect on the edge equilibrium is caused by the increased Shafranov shift that makes the flux surfaces more tightly packed on the low-field side. The shift lowers the inverse aspect ratio ($\epsilon = a/R$) on the outboard side. Since the ratio of trapped to passing particles is approximately $\sqrt{2\epsilon}/(1+\epsilon)$, it is also reduced with increasing Shafranov shift. The decreasing fraction of trapped particles lowers the flux surface averaged bootstrap current $\langle \boldsymbol{j} \cdot \boldsymbol{B} \rangle_{bs}/(\mu_0 J)$ that dominates the inductively driven current in the edge region. Figure 8 illustrates how the toroidal current profile at the midplane varies with β_p. The current peak on the low-field side is reduced with increased β_p.

We integrate the current density over the poloidal cross-section area between two flux surfaces and then differentiate with respect to ψ_N to get $\mathrm{d}I/\mathrm{d}\psi_N(\psi_N)$, where I is the toroidal current. The edge profile of $\mathrm{d}I/\mathrm{d}\psi_N(\psi_N)$ is plotted in figure 9. The reason for the lower toroidal current at high β_p is the following. First, as explained above, the flux surface averaged current is reduced by the smaller trapped to passing particle ratio. Second, since the flux surfaces on the low-field side are closer together, the poloidal cross-section area between two flux surfaces is also reduced there. At same time, the area between flux surfaces on the high-field side is increased, but since the toroidal current density is much higher on the low-field side, its contribution to the total current between two flux surfaces is much smaller than that of the low-field side. Consequently, the integrated toroidal edge current between two flux

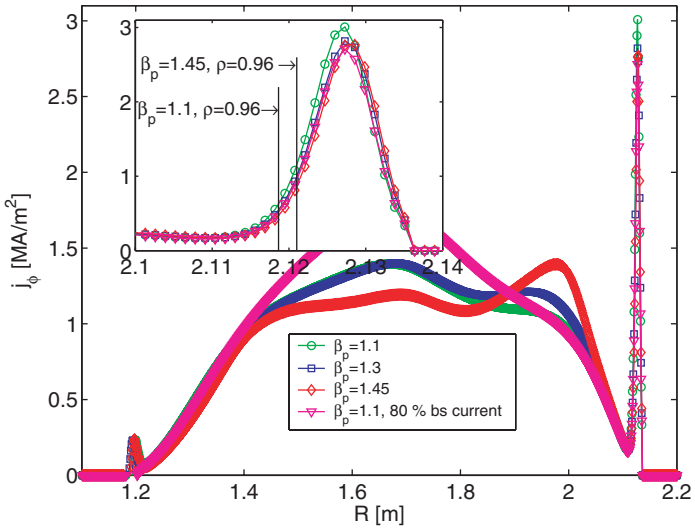

Figure 8. The toroidal current density at the midplane for three values of β_p with 100% bootstrap current taken into account in the equilibrium calculation. In addition, the profile for $\beta_p = 1.1$ with 80% bootstrap current is plotted. The inset shows the toroidal current near the low-field side edge and the $\rho = 0.96$ flux surface position illustrating the squeezing of the flux surfaces.

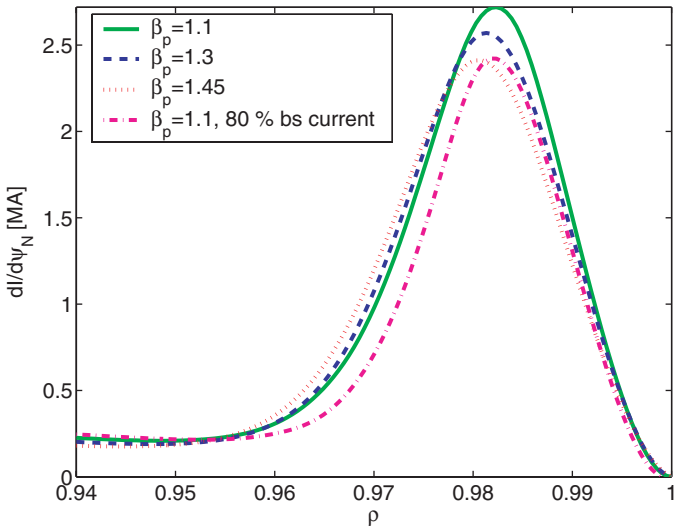

Figure 9. The flux averaged toroidal current density $\mathrm{d}I/\mathrm{d}\psi_N$ in the edge region for four values of global β_p.

surfaces is reduced with increasing β_p. However, as can be seen in figure 10, the q-profile in the edge region varies little with β_p.

In plasmas with high triangularity, in addition to the reduction of the current, the shifting of the flux surfaces makes the curvature of the magnetic field more 'favourable' in the edge region, i.e. the average $\kappa \cdot \nabla p$ decreases. This is shown in figure 11, where $\langle \kappa \cdot \nabla p \rangle$ is plotted as a function of the radius. The averaging is done along the field line around the poloidal plane.

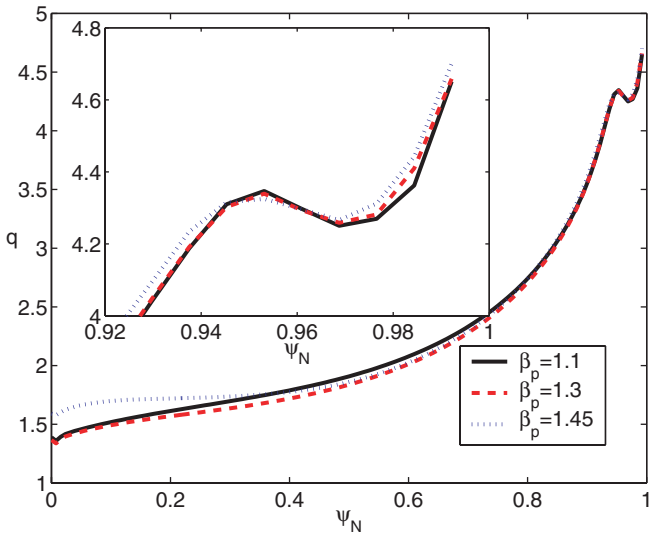

Figure 10. q-profile for various values of β_p.

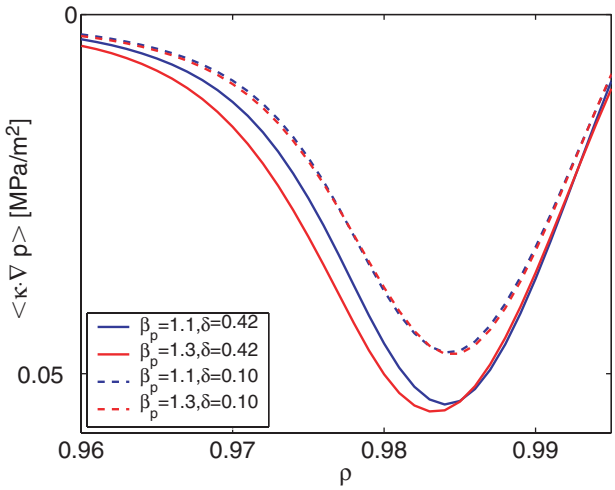

Figure 11. The driving term of the pressure driven modes ($\kappa \cdot \nabla p$) averaged over the poloidal angle along the field line for high ($\delta = 0.42$) and low ($\delta = 0.1$) triangularities.

Since the low-n peeling–ballooning modes are localized in the edge (as was shown in figure 5), the decreasing edge current and more favourable curvature with increasing β_p has a stabilizing effect on these modes as can be seen in figure 12. The plot shows the growth rates of the $n = 3$ and $n = 8$ peeling–ballooning modes as a function of the bootstrap current fraction for various values of β_p. With increasing β_p the stability boundary moves to higher values of the bootstrap current, i.e. more bootstrap current is required for the destabilization of the plasma at high β_p than at low β_p. With sufficiently high β_p, both modes can be stabilized even with 100% bootstrap current.

With the increasing mode number the ballooning (pressure driven) character of the mode becomes more dominating. Therefore, the edge current has to be lowered more to stabilize

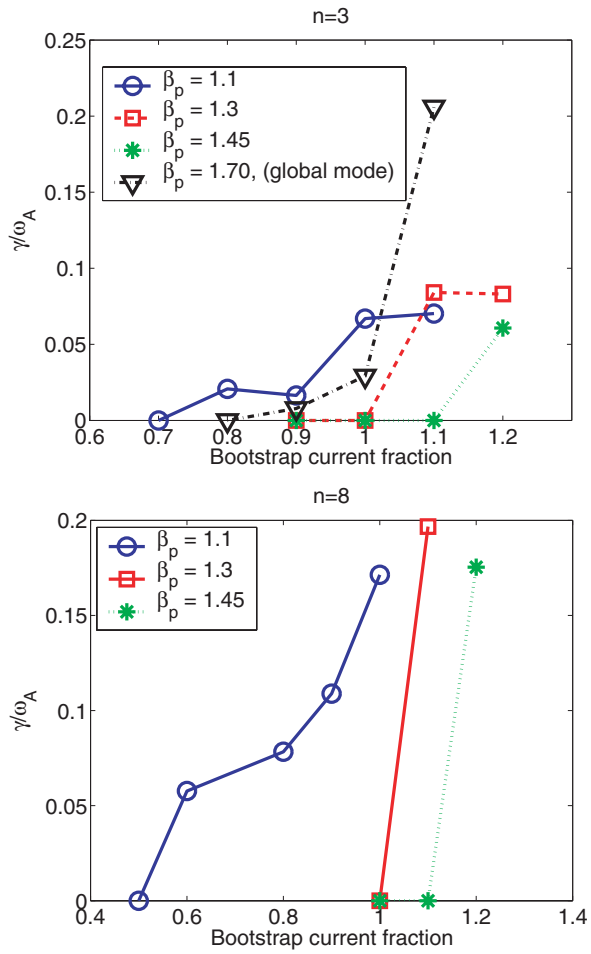

Figure 12. Growth rate of the $n = 3$ and $n = 8$ peeling–ballooning modes for the plasma with high triangularity ($\delta = 0.42$) as a function of the bootstrap current fraction for various values of β_p.

the mode with the lowest value of β_p. Also, the growth rates of the unstable high-n modes are higher than those of low-n modes, but on the other hand, the high-n modes are stabilized to some extent by the finite gyro radius stabilization whose effect is proportional to the mode number [9–11]. Unfortunately, this effect cannot be taken into account in GATO calculations.

With very high β_p (in this case $\beta_p = 1.7$), a global mode appears. It is a core mode that is driven by the current at the steep pressure gradient region of the ITB. The radial mode structure of this mode is shown in figure 13. It gives the limit of how much the edge stability can be improved by increasing the core pressure.

3.2. The effect of plasma shape

In earlier studies of ELMy ASDEX Upgrade plasmas [12,13], the plasma triangularity has been found to improve the plasma stability against the low-n peeling–ballooning modes. We analyse the stability of the equilibria with the same plasma profiles as above but with a different plasma shape to investigate how the triangularity affects the stabilizing effect of the high core pressure.

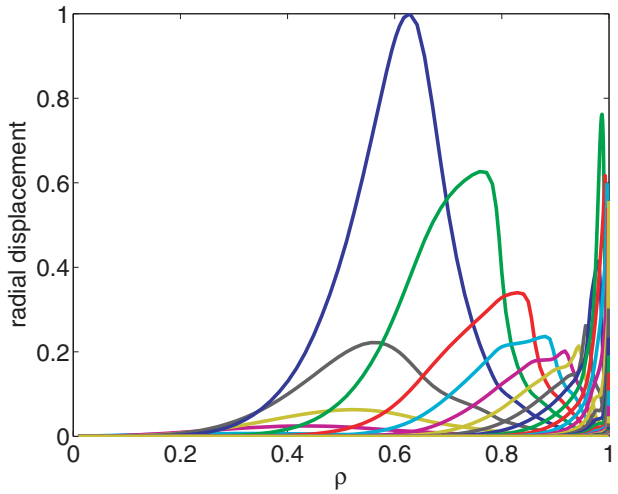

Figure 13. Fourier decomposition of the $n = 3$ peeling–ballooning mode displacement $X = \xi \cdot \nabla \psi$ in the plasma with $\beta_p = 1.7$.

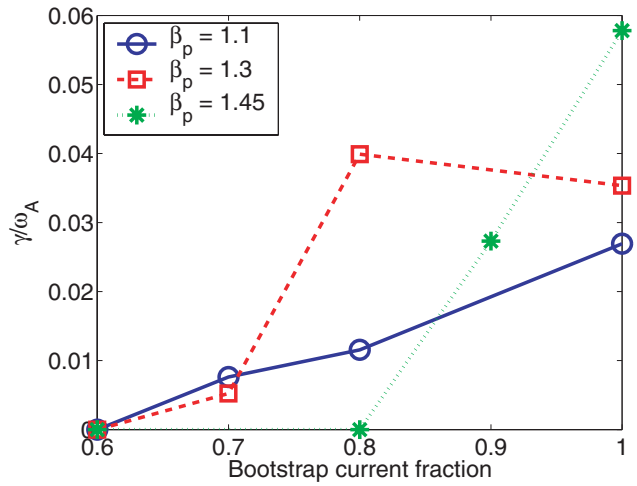

Figure 14. Growth rate of the $n = 3$ peeling–ballooning mode for the plasma with low triangularity ($\delta = 0.10$) as a function of the bootstrap current fraction for various values of β_p.

As can be seen in figure 14, at low triangularity, the low and high β_p stability boundaries are closer to each other and, thus, the stabilizing effect is reduced. The reason for the reduced stabilizing effect in low-triangularity plasmas is that the flux surface averaged favourability of the curvature, $\langle \kappa \cdot \nabla p \rangle$, is not affected by the shift of the flux surfaces like in high-triangularity plasmas, as can be seen in figure 11. The only stabilizing effect from the increasing β_p is then due to the reduction of the edge toroidal current and naturally the stabilization effect becomes weaker. This agrees qualitatively with the experimental observations at JT-60U, where the improved stability is observed only at high triangularity [3].

On the other hand, the double null shape makes the plasma more stable requiring a higher bootstrap current for the destabilization for all values of β_p. The stabilizing effect of high β_p is similar to that of a normal high triangularity single null plasma.

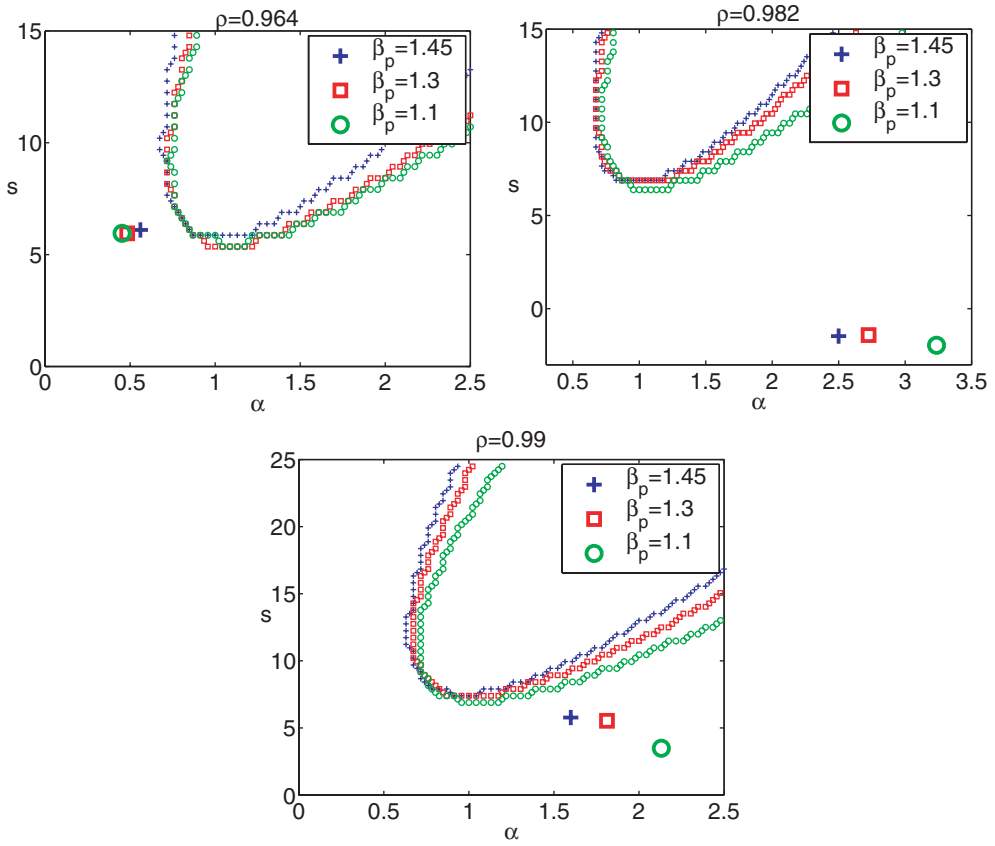

Figure 15. The $n = \infty$ ballooning mode stability boundaries (small symbols) and equilibrium values (large symbols) in shear-α space on three flux surfaces for three values of β_p.

3.3. Ballooning stability

We investigate the $n = \infty$ ballooning mode stability using IDBALL (based on methods described in [14]). Figure 15 shows the ballooning stability boundaries and the equilibrium points in the space where the normalized pressure gradient $\alpha(= -2\,\mu_0 R q^2(\mathrm{d}p/\mathrm{d}r)/B^2)$ is the x-axis and the magnetic shear $s(= \mathrm{d}q/\mathrm{d}r\, r/q)$ is the y-axis. The quantities are evaluated at the low-field side midplane. The ballooning stability is evaluated at three radial positions: at the top of the pedestal ($\rho = 0.964$), at the location of the steepest pressure gradient ($\rho = 0.982$) and between the steepest region and the plasma edge ($\rho = 0.99$), and 100% of the bootstrap current is taken into account in all the equilibria. The increasing β_p moves the equilibrium point closer to the $n = \infty$ ballooning stability boundary, but at the steepest pressure gradient region, all plasmas still have access to the second stability region.

4. Summary and discussion

For the high triangularity plasmas, the MHD stability of the edge plasma against the low-n peeling–ballooning modes was shown to improve with fixed edge parameters as the core pressure was increased. This is due to the decrease of the edge current and the more favourable

average curvature. The stabilizing effect is smaller with low-triangularity plasmas. For the $n = \infty$ ballooning mode the change in stability with global β_p is smaller. The equilibrium moves closer to the high-n ballooning stability boundary as β_p increases.

Since we used a linear code in the analysis, the non-linear behaviour of the instabilities was not investigated. Therefore, it is not possible to interpret exactly how the ELM phenomenon changes with increasing β_p. However, the improved edge stability of the high-β_p plasmas with high triangularity, would certainly have an effect on the ELM cycle. Because of the improved stability, higher edge pressure gradients (that drives the destabilizing bootstrap current) should be attainable before the ELM crash. This agrees with experimental observations.

Since the stability against low-n modes is improved with increasing β_p and at the same time the equilibrium moves closer to the high-n stability boundary, it is likely that the instability that eventually triggers ELMs in the high-β_p plasma has a higher mode number than in the low-β_p plasma. As was shown in figure 5, the increase in the mode number makes the radial width of the instability narrower. Assuming that the ELM size is proportional to the radial width of the triggering instability, the increase in the mode number of the triggering instability could explain why the observed access to smaller ELMs is facilitated with the increase of β_p.

References

[1] Connor J W, Hastie R J and Wilson H R 1998 *Phys. Plasmas* **5** 2687
[2] Saarelma S, Günter S, Kurki-Suonio T and Zerhfeld H-P 2000 *Plasma Phys. Control. Fusion* **42** A139
[3] Kamada Y *et al* 2002 *Plasma Phys. Control. Fusion* **44** A279
[4] Kamada Y *et al* 2000 *Plasma Phys. Control. Fusion* **42** A247
[5] Lao L L *et al* 2001 *Nucl. Fusion* **41** 295
[6] Sauter O, Angioni C and Lin-Liu Y R 1999 *Phys. Plasmas* **6** 2834
[7] Bernard L C, Helton F J and Moore R W 1981 *Comput. Phys. Commun.* **24** 377
[8] Maraschek M *et al* 1998 *Proc. 25th European Physical Society Conf. on Controlled Fusion and Plasma Physics (Prague)* (European Physical Society) p 492
[9] Rogers B N and Drake J F 1999 *Phys. Plasmas* **6** 2797
[10] Hastie R J, Catto P J and Ramos J J 2000 *Phys. Plasmas* **7** 4561
[11] Huysmans G T A, Sharapov S E, Mikhailovskii A B and Kerner W 2001 *Phys. Plasmas* **8** 4292
[12] Saarelma S, Guenter S and Kurki-Suonio T, Zehrfeld H-P 2000 *Plasma Phys. Control. Fusion* **42** A139
[13] Saarelma S, Guenter S and Horton L D and ASDEX Upgrade Team 2003 *Nucl. Fusion* **43** 262
[14] Connor J W, Hastie R J and Taylor J B 1979 *Proc. R. Soc. Lond. A.* **365** 1